# Spectroscopic evidence for a lava fountain driven by previously accumulated magmatic gas

**Patrick Allard[1,2], Mike Burton[1] & Filippo Muré[1]**

[1]*INGV, Piazza Roma 2, 95123 Catania, Italy*
[2]*Laboratoire Pierre Süe, CNRS-CEA, CE-Saclay, 91191 Gif sur Yvette, France*

**Lava fountains are spectacular continuous gas jets, propelling lava fragments to heights of several hundred metres, which occasionally occur during eruptions of low-viscosity magmas[1–5]. Whether they are generated by the effervescent disruption of fast-rising bubbly melt[2–5] or by the separate ascent of a bubble foam layer accumulated at depth[6,7] still remains a matter of debate[8]. No field measurement has yet allowed firm discrimination between these two models. A key insight into the origin of lava fountains may be gained by measuring the chemical composition of the driving gas phase. This composition should differ markedly depending on whether the magma degassing occurs before or during eruption[9,10]. Here we report the analysis of magmatic gas during a powerful (250–600 m high) lava fountain, measured with Fourier transform infrared spectroscopy[11–14] on Mount Etna, Sicily. The abundances of volcanic gas species, determined from absorption spectra of lava radiation, reveal a fountain gas having higher $CO_2$/S and S/Cl ratios than other etnean emissions[14–18], and which cannot derive from syn-eruptive bulk degassing of Etna basalt[19,20]. Instead, its composition suggests violent emptying of a gas bubble layer previously accumulated at about 1.5 km depth below the erupting crater.**

Lava fountains have been principally described and studied on hotspot Hawaiian volcanoes[1–5], but are also observed on basaltic and alkaline volcanoes in other tectonic settings, such as Mount Etna, in Sicily. In January–June 2000, the Southeast summit crater (SEC, 3,250 m above sea level) of Etna produced an exceptional series of 64 periodic lava fountaining episodes, with heights ranging from 80 to 900 m (ref. 21). These events, separated by quiescent intervals of 3 h to 10 days, had a reproducible pattern, and were associated with sharp peak increases of the seismic tremor[21]. The sixty-third eruptive episode, on 14 June 2000, was the best studied one[22]. After 13 h of precursory effusive then strombolian activity, it culminated with 40 min of fire fountaining that progressively increased in height from 250 to ~600 m, before ending abruptly.

During this event we could remotely measure the composition of the magmatic gas phase, by operating an open-path Fourier transform infrared (OP-FTIR) spectrometer (see Methods) at 990 m slanting distance from the south rim of SEC (Fig. 1a). OP-FTIR spectroscopy has recently been applied to analyse volcanic fumaroles[11] and plumes[12–14], but not yet a lava fountain. The fountain, several tens of metres wide, consisted of a red-orange core of incandescent gas and molten lava clots (~1,100 °C), surrounded by a darker envelope of finer pyroclasts (cinders, lapilli) and gas (Fig. 1b). The 7.5-mrad field of view of our telescope allowed us to target an ~8-m-wide area of this outer layer while collecting one FTIR spectrum every ~7 s. The 91 spectra collected during the fountain growth and climax (09:18 to 09:43 GMT) were pure absorption spectra, demonstrating that pyroclasts in the targeted area were always hotter than the coexisting volcanic gas. The mean temperature of these radiating clasts, determined by spectral fitting with a scaled Planck curve, varied between 510 and 630 °C, compared with 450 ± 25 °C for the gas, as inferred from the rotational band structure of the $SO_2$ absorption. Such moderate temperatures demonstrate extensive cooling of both solid particles and volcanic gas in the outer part of a lava fountain, owing to radiative cooling and air entrainment[2,5].

The identity and molar path amount (in molecules per $cm^2$) of each gas species along the beam path length were determined from spectral absorption lines of the infrared radiation emitted by pyroclasts. In each spectrum we detected eight gas species—namely $H_2O$, $CO_2$, $SO_2$, $CH_4$, $N_2O$, HCl, HF and CO (given in order of decreasing abundance). Whereas $N_2O$ is purely atmospheric and $SO_2$, HCl and HF are purely volcanic, the other four species are present both in volcanic emissions and in air. Their amounts were thus corrected for the atmospheric amount of each species along the beam path length, derived from the *y*-intercept of regression lines of scatter plots versus $SO_2$ and/or HCl (ref. 12). The gradients of regression lines provide the mean volcanic gas ratios presented below. The mean air concentrations inferred at ambient pressure (~680 hPa) and temperature (15 °C) of the measurement—7,700 parts per million by volume, p.p.m.v., $H_2O$ (~30% relative

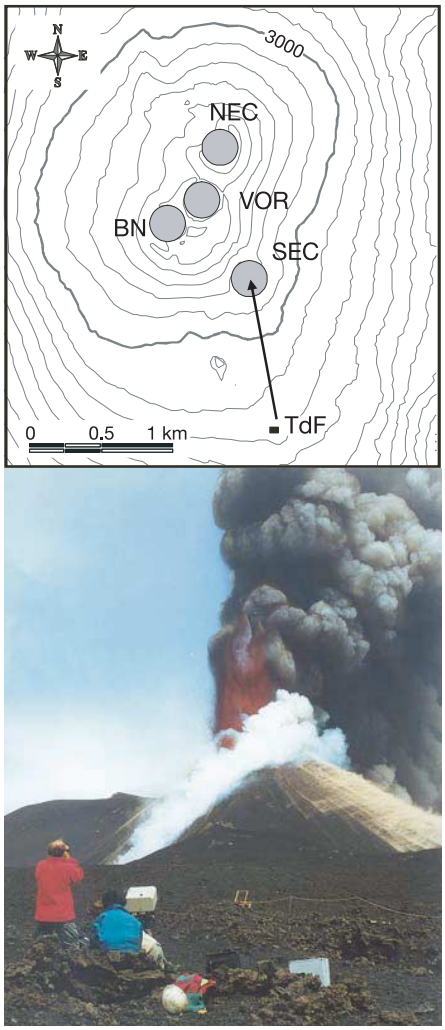


**Figure 1** OP-FTIR measurement of the 14 June 2000 lava fountain on Etna. The sketch map shows the measuring site location, at 2,900 m elevation south of Southeast summit crater (SEC). TdF, Torre del Filosofo alpine shelter. VOR, BN and NEC denote Voragine, Bocca Nuova and Northeast summit craters, respectively. Beam path length is 990 m (arrow). The picture (35° angle view) shows the lava fountain at 09:28 GMT, when it was ~300 m high and lava had begun overflowing the south crater rim (whitish fumes in the foreground). The FTIR spectrometer is targeting an 8-m-wide area of the fountain about 70 m above the crater, in order to minimize interference from the whitish fumes.

humidity), 364 p.p.m.v. $CO_2$, 1.9 p.p.m.v. $CH_4$ and 0.12 p.p.m.v. CO—agree well with concentrations measured on top of Etna ($H_2O$, $CO_2$)[18] and in Sicily (CO, $CH_4$)[23]. Once air background is removed, most spectra contain pure volcanic $CO_2$ and CO, but no detectable methane, in agreement with the very low abundance of that species in magmatic gas[10]. The corrected concentrations for $H_2O$ are less clear-cut: natural atmospheric variability increases their apparent error to ~20%, compared with 4–10% for other species; moreover, they can include unresolved and variable additions from air moisture entrained within the fountain, and possibly also ground water sucked into the erupting conduit. Therefore, we can only provide upper limits for the $H_2O$ content of the magmatic gas.

Figure 2 shows the evolution of the gas concentrations and ratios together with seismic tremor amplitude, a good proxy for the eruption intensity[22]. Restricted chemical variations were initially observed during fountain growth (09:23:06 to 09:26:42 GMT; Fig. 2a). The driving gas contains on average 96 mol% $H_2O$, 3.7 mol% $CO_2$, 0.4 mol% $SO_2$, 0.037 mol% HCl, 0.02 mol% HF and 0.004 mol% CO. It has high mean $CO_2/S$ (~10) and S/Cl (~10) ratios, and a low Cl/F ratio (~2). During increasingly powerful fountaining (09:28:48 to 09:40:47 GMT), the gas species displayed larger oscillations (Fig. 2a). These reflect the accelerating eruption dynamics, but also variable spectroscopic interference from whitish fumes rising from lava that started to overflow the south rim of SEC from 09:26 GMT (Fig. 1). This interference resulted in occasional sharp increases in the optical thickness of the volcanic gas layer, but is easily identified by its distinct composition (Fig. 3). In this interval, the uncontaminated fountain gas had an average composition of 92 mol% $H_2O$, 7.3 mol% $CO_2$, 1.0 mol% $SO_2$, 0.10 mol% HCl, 0.07 mol% HF and 0.004 mol% CO. It maintained a similarly high S/Cl ratio (10), but had somewhat lower $CO_2/S$ (7.3) and Cl/F (1.3) ratios than during the previous stage. We assessed its equilibrium temperature from the $CO/CO_2$ ratio and standard thermodynamic data for the reaction $2CO+O_2=2CO_2$, assuming gas–melt equilibrium under redox conditions (log $f_{O_2} \approx$ NNO+0.3, where NNO is the nickel–nickel oxide oxygen buffer) typical for Etna basalt[15,24]. This leads to: $T = -2{,}330/[\log(CO/CO_2)+0.357] - 273$, where $T$ is in °C. The computed mean values of 640 ± 30 °C and 530 ± 70 °C for the two periods described above are higher than the physical gas temperature (450 ± 25 °C) inferred from $SO_2$ rotational structure, and close to the estimated Planck temperature of radiating pyroclasts (Fig. 2b), indicating efficient compositional quenching of the gas upon cooling.

Between 09:45 and 09:57 GMT we obtained a further 90 spectra of post-fountaining magma degassing at the south crater rim. In these emissions, only volcanic $SO_2$, HCl and HF were detected. The observed gradual decrease of S/Cl (from ~3.5 to 1) and Cl/F (from 1.3 to 0.9) ratios, along with declining activity (Fig. 2b), demonstrates a preferential exhaustion of $SO_2$ relative to HCl and HF during degassing of the cooling magma, as also observed

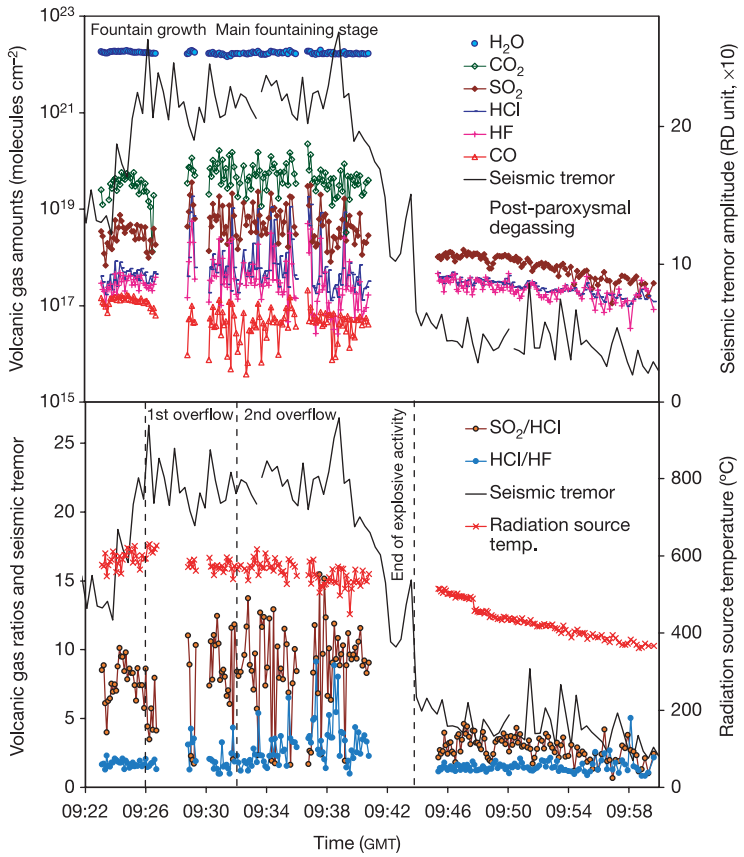


**Figure 2** Temporal evolution of volcanic gas concentrations and ratios during and after the 14 June 2000 lava fountain. Top, time series of measured path amounts of volcanic gases (left-hand log scale), together with the volcanic tremor amplitude[21,22] (right-hand scale, RD × 10: here RD indicates reduced displacement, in $cm^2$) as an indicator of the eruption intensity. $H_2O$, $CO_2$ and CO amounts are corrected for atmospheric background (see text). Bottom, evolution of $SO_2$/HCl and HCl/HF ratios (left-hand scale) during and after the fountaining, and evolution of the radiating source temperature retrieved from FTIR spectra (right-hand scale). Smooth decrease of that temperature during the main fountaining stage reflects the influence of progressive widening of the falling (cooler) tephra area along with greater height of the jets. Left and centre dashed lines indicate the onset of bursts of lava overflowing the upper south crater rim; right dashed line indicates end of explosive activity.

from etnean lava flows[14,15]. $SO_2$ was no longer detected in residual, HF-dominated emanations from the flowing lava, measured between 10:25 and 11:03 GMT.

Our data thus provide a detailed record of the chemical evolution of magmatic gas during and after a powerful lava fountain on a basaltic volcano. Before our study, one single spectroscopic datum had been obtained[25] in 1968 for $H_2O$, $CO_2$ and $SO_2$ during 10-m-high lava spattering on Kilauea volcano, in Hawaii. Compared with other etnean emissions[14–18], the fountain gas analysed here shows remarkable compositional features, which allow us to elucidate its genesis by reference to data for dissolved volatiles in Etna magma[19,20,24,26]. Its high $H_2O$ content and low $CO_2/H_2O$ ratio (0.04–0.08) are not particularly unusual[15], as etnean gases arise from exceptionally water-rich basalts (3.4 wt%)[19]. However, the significance of these two parameters is limited by the above-mentioned, quite large, uncertainties on $H_2O$. In contrast, the $CO_2/S$ and S/Cl ratios of the fountain are highly discriminating. Both are 2 to 4 times higher than the representative ratios for time-averaged Etna plume emissions (~3 and 2–4, respectively[14,15,18]; Fig. 3) and no such S/Cl ratio has previously been measured in etnean eruptive gas[15]. Moreover, these two ratios are sensitive tracers of Etna basalt decompression and degassing[15,19,20]. During magma ascent, carbon dioxide exsolves much earlier than sulphur, and sulphur earlier and more extensively than chlorine, this evolution being best documented for S and Cl[19,20]. The coexisting bulk gas phase thus evolves from very high $CO_2/S$ and S/Cl ratios at high pressure down to low (molar) ratios of ~3 at atmospheric pressure[14,18–20]. Therefore, a lava fountain driven by syn-eruptive bulk magma degassing is expected to display $CO_2/S$ and S/Cl ratios of ~3, whereas previous gas–melt separation at depth should result in higher ratios.

Clearly, our results do not support a bulk degassing process and instead indicate gas-melt separation. We cannot exclude the possibility that degassing of fast-rising basalt could favour high S/Cl ratios owing to a lower diffusivity of chlorine relative to sulphur. However, the constant S/Cl ratio of the fountain gas, despite large variations in eruptive velocities[22], as well as the lack of anomalous residual Cl content in the erupted tephra (P.A. *et al.*, manuscript in preparation), point to a minor influence of such late-stage kinetic effects. Moreover, earlier exsolved carbon dioxide and sulphur should be much less sensitive to such effects than more soluble HCl. Consequently, the presence of both high $CO_2/S$ and S/Cl ratios in the fountain (Fig. 3) strongly argues in favour of a prevalent control of the gas composition by gas–melt separation at depth. The measured S/Cl ratio of ~10 corresponds to bulk equilibrium with Etna basalt under pressures of the order of 30–40 MPa (ref. 20 and N. Spilliaert *et al.*, manuscript in preparation), implying that the erupted gas phase preserved a composition established at about 1.5 km lithostatic depth below SEC (for a mean rock density of 2,600 kg $m^{-3}$).

Hence, we conclude that the measured lava fountain was most probably driven by the separate ascent of a gas layer previously accumulated at moderate depth within the volcanic pile (3,300 m high). This conclusion is consistent with independent evidence that the eruption was supplied by a shallow magma body undergoing rapid crystallization, on top of which repeated growth and collapse of a bubble foam may have triggered periodic lava fountaining (P.A. *et al.*, manuscript in preparation). This interpretation is reminiscent of the bubble foam model[7] for periodic lava fountaining on Kilauea volcano. However, not all lava fountains are necessarily powered by this mechanism[8]. Here we demonstrate that remote gas sensing using OP-FTIR spectroscopy opens new ways to better understanding of lava fountain dynamics. □

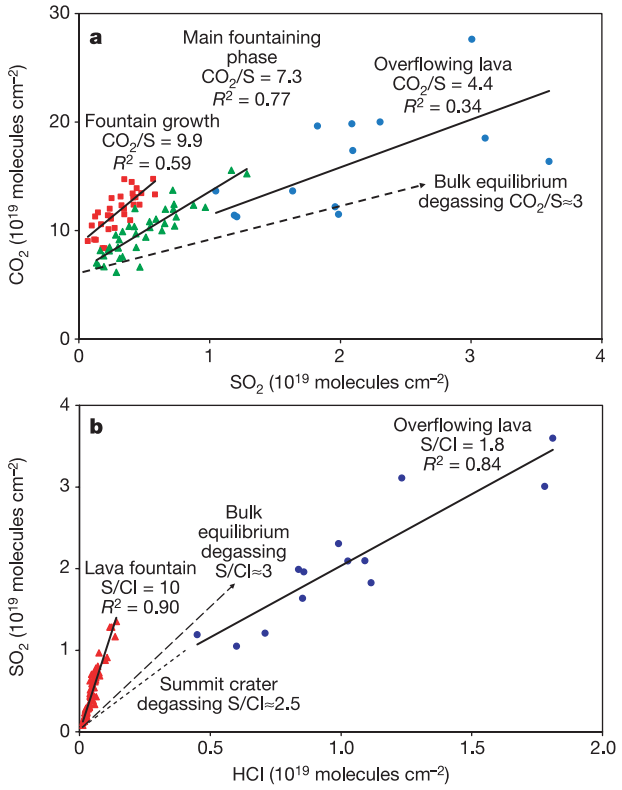


**Figure 3** Scatter plots of gas amounts measured during lava fountaining. **a**, $CO_2$ versus $SO_2$, and **b**, $SO_2$ versus HCl, showing the distinct mean volcanic ratios in fountain gas and whitish fumes from overflowing lava. Average S/Cl and $CO_2/S$ ratios for bulk degassing of Etna basalt[14,18,19] and S/Cl ratio measured in May–June 2000 summit plume emissions[27] are shown for comparison.

## Methods

Our Bruker model OPAG-22 OP-FTIR spectrometer has been operated since May 2000 for routine solar occultation measurements of Etna's summit plume composition[27]. It has a ZnSe beamsplitter, 0.5 $cm^{-1}$ spectral resolution and 1.78 cm optical path difference, and is equipped with an internal black-body calibration system. The detector used was a liquid-nitrogen-cooled InSb photovoltaic semiconductor with effective sensitivity between 1,500 and 5,000 $cm^{-1}$. Spectra were calculated from the Fourier transform of double-sided interferograms using Norton-Beer medium apodization and power spectrum phase correction. Gas concentrations were determined from spectra using a nonlinear least-squares fitting program based on the optimal estimation algorithm[28] and infrared absorption parameters from the HITRAN 96 spectral database[29]. We considered a two layer model of atmospheric (15 °C) and volcanic gases (80 °C for lava fumes, 450 °C for fountain gas), calculated from the RFM radiative transfer code (http://www-atm.atm.ox.ac.uk/RFM). The volcanic gas temperature was retrieved by analysing the rotational structure of the $SO_2$ absorption. The uncertainty due to measurement and retrieval on reported gas amounts ranges from 4% to 10%.

Received 11 July; accepted 29 November 2004; doi:10.1038/nature03246.

1. Swanson, D. A., Duffield, W. A., Jackson, D. B. & Peterson, D. B. Chronological narrative of the 1969–1971 Mauna Ulu eruption of Kilauea volcano, Hawaii. *US Geol. Surv. Prof. Pap.* **1056,** 1–59 (1979).
2. Wilson, L. & Head, J. W. Ascent and eruption of basaltic magma on the Earth and Moon. *J. Geophys. Res.* **86,** 2971–3001 (1981).
3. Head, J. W. & Wilson, L. Lava fountain heights at Pu'u'O'o, Kilauea, Hawaii: indicators of amount and variations of exsolved magma volatiles. *J. Geophys. Res.* **92,** 13715–13719 (1987).
4. Sparks, R. S. J. The dynamics of bubble formation and growth in magmas. *J. Volcanol. Geotherm. Res.* **3,** 1–37 (1978).
5. Parfitt, E. A., Wilson, L. & Neal, C. A. Factors influencing the height of Hawaiian lava fountains: implications for the use of fountain height as an indicator of magma gas content. *Bull. Volcanol.* **57,** 440–450 (1995).
6. Jaupart, C. & Vergniolle, S. Laboratory models of Hawaiian and Strombolian eruptions. *Nature* **331,** 58–60 (1988).
7. Vergniolle, S. & Jaupart, C. Dynamics of degassing at Kilauea volcano, Hawaii. *J. Geophys. Res.* **95,** 2793–2809 (1990).
8. Parfitt, E. A. A discussion of the mechanisms of explosive basaltic eruptions. *J. Volcanol. Geotherm. Res.* **134,** 131–144 (2004).
9. Gerlach, T. M. Exsolution of $H_2O$, $CO_2$, and S during eruptive episodes at Kilauea Volcano, Hawaii. *J. Geophys. Res.* **91,** 12177–12185 (1986).

10. Giggenbach, W. F. In *Monitoring and Mitigation of Volcano Hazards* (eds Scarpa, R. & Tilling, R.) (Springer, Berlin, 1996).
11. Mori, T. *et al.* Remote detection of fumarolic gas chemistry at Vulcano, Italy, using an FT-IR spectral radiometer. *Earth Planet. Sci. Lett* **134,** 219–224 (1995).
12. Francis, P. W., Burton, M. & Oppenheimer, C. Remote measurements of volcanic gas compositions by solar FTIR spectroscopy. *Nature* **396,** 567–570 (1998).
13. Burton, M., Oppenheimer, C., Horrocks, L. A. & Francis, P. W. Field measurement of $CO_2$ and $H_2O$ emissions from Masaya Volcano, Nicaragua, by Fourier transform spectrometry. *Geology* **28,** 915–918 (2000).
14. Burton, M., Allard, P., Murè, F. & Oppenheimer, C. In *Volcanic Degassing* (eds Oppenheimer, C., Pyle, D. & Barclay, J.) 281–293 (Special Publication 2213, Geological Society, London, 2003).
15. Allard, P. *Géochimie Isotopique et Origine de l'eau, du Carbone et du Soufre dans les Gaz Volcaniques: Zones de Rift, Marges Continentales et Arcs Insulaires*. Thesis, Paris 7 Univ. (1986).
16. Allard, P. *et al.* Eruptive and diffuse emissions of carbon dioxide from Etna volcano. *Nature* **351,** 387–391 (1991).
17. Pennisi, M. & Le Cloarec, M. F. Variations of Cl, F, and S in Mount Etna's plume, Italy, between 1992 and 1995. *J. Geophys. Res. B* **103,** 5061–5070 (1998).
18. Allard, P. *Monitoring Volcanic Risk by Remote Sensing Techniques: Airborne Plume Validation* (Final Rep. MVRRS RTD Contract, ENV4960288, CEE-DGXII, Bruxelles, 1999).
19. Métrich, N., Allard, P., Spilliaert, N., Andronico, D. & Burton, M. 2001 flank eruption of the alkali- and volatile-rich primitive melt responsible for Mount Etna's evolution in the last three decades. *Earth Planet. Sci. Lett.* **228,** 1–17 (2004).
20. Spilliaert, N., Allard, P., Métrich, N. & Sobolev, A. A new step in modelling magma degassing processes and eruptive dynamics at Mount Etna: the 2002–2003 eruption. *Geophys. Res. Abstr.* **6,** 04189 (2004).
21. Alparone, S., Andronico, D., Lodato, L. & Sgroi, T. Relationship between tremor and volcanic activity during the Southeast Crater eruption on Mount Etna in early 2000. *J. Geophys. Res.* **108,** 2241, doi:10.1029/2002JB001866 (2003).
22. Allard, P. *et al.* Source process of cyclic fire fountaining at Mt. Etna in 2000: a multidisciplinary study of the June 14 (63rd) event. *Geophys. Res. Abstr.* **5,** 13079 (2003).
23. World Data Centre for Greenhouse Gases, Japan Meteorological Agency. http://gaw.kishou.go.jp/wdcgg.html.
24. Métrich, N. & Clocchiatti, R. Sulfur abundance and its speciation in oxidized alkaline melts. *Geochim. Cosmochim. Acta* **60,** 4151–4160 (1996).
25. Naughton, J. J., Derby, J. V. & Glover, R. B. Infrared measurements on volcanic gas and fume: Kilauea eruption, 1968. *J. Geophys. Res.* **74,** 3273–3277 (1969).
26. Métrich, N., Clocchiatti, R., Mosbah, M. & Chaussidon, M. The 1989–1990 activity of Etna magma mingling and ascent of $H_2O$-Cl-S-rich basaltic magma. Evidence from melt inclusions. *J. Volcanol. Geotherm. Res.* **59,** 131–144 (1993).
27. Allard, P., Burton, M., Brusca, L. & Murè, F. *Geochemical Monitoring of Sicilian Volcanoes* (Second Rep., July-December 2000, Sistema Poseidon, Nicolosi, Italy, 2000).
28. Rodgers, C. D. Retrieval of atmospheric temperature and composition from remote measurements of thermal radiation. *Rev. Geophys. Space Phys.* **14,** 609–624 (1976).
29. Rothman, L. S. *et al.* The HITRAN molecular spectroscopic database and HAWKS (HITRAN Atmospheric Workstation): 1996 edition. *J. Quant. Spectrosc. Radiat. Transfer* **60,** 665–710 (1998).

**Acknowledgements** We thank F. Barberi and L. Villari for their initial support of the Etna FTIR monitoring project within the Poseidon System (Italian Civil Defence and Sicily Region), and A. Bonaccorso, E. Boschi and S. Calvari for their continued support within INGV. We acknowledge early technical assistance from the Bruker company (Germany) and discussions with N. Métrich (LPS) and our colleagues in INGV-Catania.

**Competing interests statement** The authors declare that they have no competing financial interests.

**Correspondence** and requests for materials should be addressed to P.A. (patrick.allard@cea.fr).

# Long-term relationships between ecological stability and biodiversity in Phanerozoic reefs

**Wolfgang Kiessling**

*Museum of Natural History, Humboldt University Berlin, Invalidenstrasse 43, D-10115 Berlin, Germany*

**High biodiversity has been shown to enhance ecological stability on small spatial scales and over intervals of weeks to decades[1–4]. It remains unclear, however, whether this diversity–stability relationship can be scaled up to regional scales, or to longer timescales[5]. Without empirical validation at larger scales, the implications of the diversity–stability relationship for both ecology and long-term conservation strategies cannot readily be resolved. Here I show that in biogenic reefs, ecological stability is related to taxonomic diversity on million-year timescales. The higher the mean reef diversity in a particular time interval, the smaller the change in skeletal density, style of reef building and biotic reef types in the subsequent time interval. Because the relationships apply to a wide spectrum of disturbance regimes and reef types, these results support the hypothesis that species richness itself promotes ecological stability[3]. Carbonate production by reefs, while closely correlated with reef diversity without temporal lag, is not stabilized by reef diversity over these long timescales. This suggests that ecological stability and productivity may be decoupled in natural ecosystems.**

Reefs, broadly defined as laterally confined structures built by the growth and/or metabolic activity of sessile benthic organisms in an aquatic environment, are an excellent tool for tracking long-term ecological changes, because they have an outstanding fossil record reaching back at least two billion years and because they yield a number of attributes, other than taxonomic richness, that permit the identification of ecological traits. Reefs changed substantially in abundance, composition, palaeogeographic distribution, geometric attributes and biodiversity during the Phanerozoic eon (the past 542 million years, Myr), but these changes are rarely linearly correlated with global environmental changes—at least as inferred from the geological record[6,7]. Biological controls seem either to buffer the reef system (the combined traits of all reefs recorded within a time interval) or to amplify responses to global change on timescales of millions of years[7,8]. Using a database of more than 3,300 Phaner-

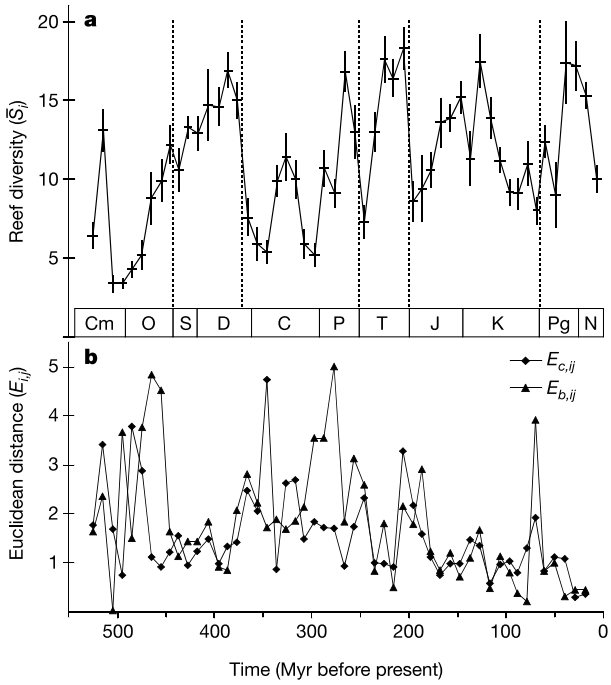


**Figure 1** Time series of mean reef diversity and two measures of ecological change resolved to 10-Myr intervals. **a**, Reef diversity expressed as the mean species richness (number of species) of reef-builders within individual reef complexes per time interval. Vertical bars indicate one standard error of the mean in each direction. Horizontal bars demarcate the spans of time intervals. Vertical dashed lines mark the big five mass extinction events of the Phanerozoic. Cm, Cambrian; O, Ordovician; S, Silurian; D, Devonian; C, Carboniferous; P, Permian; T, Triassic; J, Jurassic; K, Cretaceous; Pg, Paleogene; N, Neogene. **b**, Ecological changes between consecutive time intervals (*i*–*j*, plotted in *i*) expressed as the euclidean distances of constructional styles ($E_{c,ij}$) and biotic reef types ($E_{b,ij}$).